Non-Classical Thermal Physics in Force-Driven Micro-Channel Gas Flows

Rho Shin MYONG [1,*]

* Corresponding author: Tel.: +82-55-772-1645; Fax: +82-55-772-1580; Email: myong@gnu.ac.kr
1 Department of Aerospace and System Engineering and Research Center for Aircraft Parts Technology,
Gyeongsang National University, South Korea

Abstract The fundamental physics of non-classical thermal characteristics in micro-channel gas flows is investigated on the basis of non-Fourier law embedded in moment equations derived from the kinetic Boltzmann equation. First, the effects of the force-stress coupling term on thermal behavior are examined in both Navier non-Fourier and non-Navier non-Fourier laws. It is shown that the ultimate source behind the non-monotonic temperature distribution is the force-stress coupling term in the constitutive equation of heat flux, irrespective of the constitutive equations of viscous stress, classical or non-classical. Second, the thermal characteristics such as the temperature and heat flux distributions for various Knudsen numbers are investigated in order to understand the complex interaction between the force and the rarefaction effects. It is shown that the central temperature reaches minimum in whole flow field after a critical Knudsen number in case of non-Navier non-Fourier law. Lastly, it is demonstrated that the force-stress coupling term in the non-Fourier law is solely responsible for the so-called Knudsen minimum of mass flow rate in the force-driven compressible Poiseuille gas flow, which is against intuition obtained from classical theory and indicates a dominant role of non-classical thermal physics in gas flow far from thermal nonequilibrium.

Keywords: micro gas flow, non-Fourier law, thermal characteristics

1. Introduction

The study of flow and thermal characteristics of gases associated with micro- and nano-devices remains as an important scientific topic. Previous studies (Bhattacharya and Lie, 1989; Tij and Santos, 1994; Mansour et al., 1997; Uribe and Garcia, 1999; Zheng et al., 2002; Xu, 2003; Karniadakis et al., 2005) had revealed that the fundamental physics in micro- and nano-scale gases is significantly different from the physics valid in conventional macro-scale flows. For instance, it was shown by various studies that the classical Navier-Fourier laws cannot predict the correct flow physics of the force-driven Poiseuille gas flow. In particular, the classical theory was not able to describe the non-monotonic temperature distribution across a micro-channel (Tij and Santos, 1994; Mansour et al., 1997).

The one-dimensional force-driven (or acceleration-driven) compressible Poiseuille gas flow depicted in Fig. 1 is defined as a stationary flow in an infinitely long channel under the action of a constant external force parallel to the walls. In a previous study based on a nonlinear coupled constitutive relation (NCCR) (Myong, 2011) derived from the Boltzmann equation via the moment method (Myong, 2014), it was shown that the term of coupling of force and viscous shear stress appearing in the constitutive equation of heat flux is responsible for the unusual feature of the central temperature minimum, which is in stark contrast with conventional monotonic quartic profile. However, there remain some unresolved issues, such as how the coupling of force and shear stress in the non-Fourier thermal law can affect the flow and thermal characteristics when it is combined with the Navier fluid dynamic law.

In the present study, the fundamental physics, in particular, non-classical thermal characteristics in micro-channel gas flows is investigated on the basis of non-Fourier law embedded in NCCR. The effects of the force-stress coupling term on thermal behavior are

examined in detail in both classical Navier and non-classical non-Navier framework. In particular, an emphasis will be placed on the ultimate source behind the non-monotonic temperature distribution. In addition, the thermal characteristics such as the temperature and heat flux distributions for various Knudsen numbers will be investigated in order to understand the complex interaction between the force and the rarefaction (or the size of the channel) effects. Further, other important exotic features in the force-driven compressible Poiseuille gas flow, such as non-uniform pressure distribution and non-zero normal stress, will be explained. Lastly, it will be demonstrated that the so-called Knudsen minimum in mass flow rate is directly related to the non-classical thermal behavior due to the force-stress coupling term. In other words, the increase of average temperature within the channel after a threshold Knudsen number in transitional regime is solely responsible for the minimum, indicating a dominant role of thermal aspects on general flow physics in non-classical gas flow regimes.
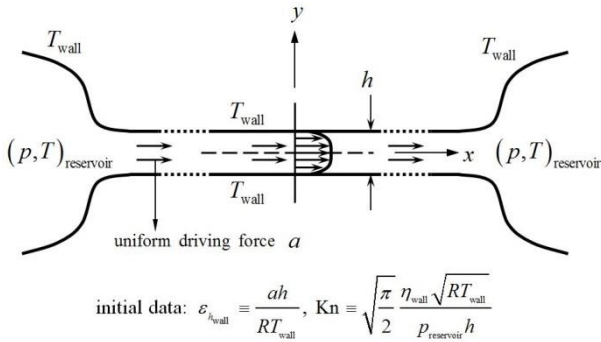
Fig. 1. Schematic of the one-dimensional fully-developed compressible Poiseuille gas flow driven by uniform force in rectangular channel between two pressure-regulated reservoirs.

2. Non-Classical Thermal Physics in Force-Driven Poiseuille Gas Flows

2.1 Non-Fourier law combined with Navier law

A mathematical technique for taking into account temperature variation of viscosity and thermal conductivity coefficients in rigorous way has been developed recently by Myong

(Myong, 2011). The new technique is based on the introduction of average quantities for velocity and temperature profiles, a spatial variable scaled by the temperature, and subsequent auxiliary relations. It employs average quantities u_r and T_r defined as

$$u_r = \frac{2}{h}\int_0^{h/2} u\, dy, \quad T_r = \frac{h/2}{\int_0^{h/2} T^{-1} dy}, \qquad (1)$$

and with the introduction of a new variable s defined as ($s^* = sT_r/h$)

$$Tds = dy \quad \text{or} \quad T^* ds^* = dy^*, \qquad (2)$$

the following auxiliary relations can be derived:

$$s^*\left(y^* = \frac{1}{2}\right) = \frac{1}{2}, \quad \int_0^{1/2} u^* T^* ds^* = \frac{1}{2}, \quad \int_0^{1/2} T^* ds^* = \frac{1}{2}. \qquad (3)$$

The conservation laws of the present force-driven compressible Poiseuille gas flow,

$$\frac{d}{dy}\begin{bmatrix} \Pi_{xy} \\ p + \Pi_{yy} \\ \Pi_{yz} \\ \Pi_{xy}u + Q_y \end{bmatrix} = \begin{bmatrix} \rho a \\ 0 \\ 0 \\ \rho a u \end{bmatrix}, \qquad (4)$$

are then solved first in term of the variable s and later transformed into the y-coordinate. The x-momentum equation in conservation laws, together with the equation of state, $p = \rho RT$, is reduced as follows:

$$\frac{d\Pi_{xy}^*}{ds^*} = \frac{\varepsilon_h}{N_\delta} \quad \text{or} \quad \Pi_{xy}^* = \frac{\varepsilon_h}{N_\delta} s^*. \qquad (5)$$

In the present problem, the following dimensionless variables and parameters are introduced:

$$y^* = y/h, \ u^* = u/u_r, \ T^* = T/T_r,$$

$$p^* = p/p_m, \ \Pi^* = \Pi/(\eta_w u_r/h),$$

$$Q^* = Q/(k_w \Delta T/h), \ \varepsilon_h = \frac{ah}{RT_r}, \ \varepsilon_{h_w} = \frac{\varepsilon_h}{T_w^*},$$

$$M = \frac{u_r}{\sqrt{\gamma RT_w}}, \ \text{Kn} = \sqrt{\frac{\pi}{2}}\frac{\eta_w \sqrt{RT_w}}{p_m h},$$

$$N_\delta = \frac{\eta_w u_r/h}{p_m}, \ \text{Ec} = \frac{(\gamma-1)M^2}{|T_m - T_w|/T_w}, \ \text{Pr} = \frac{C_p \eta_w}{k_w},$$

where the subscripts r, w and m denote the reference state, the state at the wall, and

the state at the middle of a slab, respectively. Here a denotes the external force. The parameters ε_h, M, N_δ, Kn, and Ec are dimensionless hydrodynamic numbers: a force-related number (similar to the Richardson number), Mach number, a composite number, Knudsen, and Eckert numbers, respectively. The composite number N_δ is related to other numbers such that $N_\delta = \sqrt{2\gamma/\pi}\, M$ Kn. With the assumption of Maxwell molecules, that is, $\eta(T) = \eta_w T / T_w$, and the Navier law of viscous stress,

$$\Pi_{xy}^* = -\frac{1}{T_w^*}\frac{du^*}{ds^*}, \qquad (6)$$

the velocity profile may be obtained:

$$u^*(s^*) = u^*(0) - T_w^* \frac{\varepsilon_h}{N_\delta}\frac{s^{*2}}{2}. \qquad (7)$$

With the Langmuir slip velocity condition (Myong, 2004; Myong et al., 2006; Chen and Tian, 2007; Veltzke and Thöming, 2012),

$$u^*(s^* = 1/2) = (1 - \alpha_V)u^*(s^* = 0), \qquad (8)$$

the resulting velocity profile can be expressed as

$$u^*(s^*) = u^*(0)\left(1 - 4\alpha_V s^{*2}\right)$$

where

$$\frac{T_w^*}{8}\frac{\varepsilon_h}{N_\delta} = \alpha_V u^*(0),$$

$$\alpha_V = \frac{\bar{\beta}_V}{1 + \bar{\beta}_V}, \ \bar{\beta}_V = \frac{1}{4\omega_V \mathrm{Kn}}. \qquad (9)$$

The coefficient ω_V plays a very similar role to that of the slip coefficient in the Maxwell slip model and may be assumed 1.

Non-Fourier constitutive equation of normal heat flux within linear Navier framework can be written

$$Q_y = -k\frac{dT}{dy} + \frac{ak}{pC_p}\Pi_{xy} \qquad (10)$$

where the force-stress coupling term $a\Pi_{xy}/(pC_p/k)$ originates from the acceleration term $\mathbf{a}\cdot\nabla_v f$ in the Boltzmann equation. And the energy equation in conservation laws (4) is reduced to

$$\frac{dQ_y^*}{ds^*} = \Pr \mathrm{Ec}\, T_w^* \Pi_{xy}^{*2}. \qquad (11)$$

When it is combined with equation (5) and is integrated once, the normal heat flux in the y-direction can be written as

$$Q_y^* = \frac{1}{3}\Pr \mathrm{Ec}\, T_w^* \frac{\varepsilon_h^2}{N_\delta^2}s^{*3}$$

$$\text{or} \quad \frac{Q_y}{hp^2(0)/\eta_w} = \frac{1}{3}T_w^* \varepsilon_h^2 s^{*3}. \qquad (12)$$

With the assumption of Maxwell molecules for the thermal conductivity, (10) becomes an ordinary differential equation of $T^*(s^*)$

$$\frac{dT^*}{ds^*} - ms^*T^* = -ns^{*3} \ \text{where}$$

$$m = \frac{(\gamma-1)}{\gamma}T_w^{*2}\varepsilon_{h_w}^2, \ n = \frac{1}{3}(\gamma-1)\Pr\frac{M^2}{N_\delta^2}T_w^{*5}\varepsilon_{h_w}^2,$$

$$\frac{n}{m} = \frac{\gamma}{3}\Pr\frac{M^2}{N_\delta^2}T_w^{*3} = \frac{\pi}{6}\Pr\frac{1}{\mathrm{Kn}^2}T_w^{*3}.$$
$$(13)$$

The following temperature solution can be obtained

$$T^*(s^*) = \frac{n}{m}s^{*2} + 2\frac{n}{m^2} + \left[T^*(0) - 2\frac{n}{m^2}\right]e^{\frac{1}{2}ms^{*2}}$$

and

$$\left.\frac{d^2T^*}{ds^{*2}}\right]_{s^*=0} = mT^*(0) > 0.$$
$$(14)$$

With the dimensionless temperature jump at the wall surface in the Langmuir model defined as

$$T^*(1/2) = \alpha_T T_w^* + (1 - \alpha_T)T^*(0)$$

$$= \frac{n}{4m} + 2\frac{n}{m^2} + \left[T^*(0) - 2\frac{n}{m^2}\right]e^{\frac{1}{8}m}, \quad (15)$$

$$\alpha_T = \frac{\bar{\beta}_T}{1 + \bar{\beta}_T}, \ \bar{\beta}_T = \frac{1}{4\omega_T \mathrm{Kn}},$$

the centerline temperature is then calculated using the third equation in the auxiliary relations (3):

$$T^*(0) = \frac{2n}{m^2} + \frac{\dfrac{1}{2} - \dfrac{n}{24m} - \dfrac{n}{m^2}}{F(1/2)}, F(t) \equiv \int_0^t e^{\frac{1}{2}mt^2}\,dt.$$
$$(16)$$

The average temperature T_w^* can be determined by combining it with equation (15):

$$\alpha_T T_w^* - \left(\frac{n}{4m} + \frac{2n}{m^2} - \frac{2n}{m^2} e^{m/8} \right) \tag{17}$$
$$= \left(\alpha_T - 1 + e^{m/8} \right) T^*(0).$$

The unknown value T_w^* can be easily determined in terms of initial data Kn and ε_{h_w} by a simple method such as the bisection method. Similar to the case of temperature, together with equation (16), the centerline velocity can be determined from the second equation in the auxiliary relations (3):

$$u^*(0) = \left\{ 1 - 8\alpha_v \left[\frac{1}{5 \cdot 2^5} \frac{n}{m} + \frac{2}{3 \cdot 2^3} \frac{n}{m^2} + \right. \right.$$
$$\left. \left. \left(\frac{1}{2} - \frac{n}{24m} - \frac{n}{m^2} \right) \frac{\left[e^{m/8} / 2 - F(1/2) \right]}{mF(1/2)} \right] \right\}^{-1} \tag{18}$$

Notice that the centerline velocity depends on the average temperature T_w^*. With these centerline values, the slip velocity and the temperature jump can be determined from equations (8) and (15), respectively. From the equation of state, the density profile and the average density can also be determined:

$$\rho^*(s^*) \equiv \frac{\rho}{\rho(0)} = T^*(0) \frac{p^*}{T^*} \quad \text{and}$$

$$\rho_r \equiv \frac{\int_0^{h/2} \rho dy}{h/2} = \rho(0) T^*(0). \tag{19}$$

Furthermore, the mass flow rate can be expressed as

$$\frac{\dot{m}/2h}{\rho_r \sqrt{\gamma R T_w}} \equiv \frac{\int_0^{h/2} \rho u dy}{2\sqrt{\gamma R T_w} \int_0^{h/2} \rho dy} \tag{20}$$
$$= \frac{\sqrt{\pi}}{16\sqrt{2\gamma}} \frac{T_w^{*2}}{u^*(0)} \frac{\varepsilon_{h_w}}{\text{Kn}} \frac{(1 - \alpha_V / 3)}{\alpha_V}.$$

Finally, through equation (2), that is, $y^* = \int_0^s T^*(s^*) ds^*$, all the solutions can be transformed into the domain of the distance from the wall surface y^*:

$$y^*(s^*) = \frac{n}{3m} s^{*3} + \frac{2n}{m^2} s^* + \left(\frac{1}{2} - \frac{n}{24m} - \frac{n}{m^2} \right) \frac{F(s^*)}{F(1/2)}. \tag{21}$$

2.2 Non-Fourier law combined with non-Navier law

The full analytical solutions of non-classical non-Navier non-Fourier case were already derived and validated by comprehensive DSMC results in a previous study (Myong, 2011). It was shown that the non-Navier non-Fourier theory captures all the non-classical features predicted by the DSMC calculation. The important solutions are summarized here with special emphasis on thermal features of the flow. By combining the x, y momentum equations of the conservation laws (4) and the kinematic stress constraint identified in the velocity shear flow,

$$\Pi_{xy}^2 = -\frac{3}{2} \left(p + \Pi_{yy} \right) \Pi_{yy}, \tag{22}$$

the following solutions for the pressure and stresses can be obtained:

$$p^*(S^*) = 1 + \tan^2 S^*,$$
$$\Pi_{yy}^*(S^*) = -\frac{1}{N_\delta} \tan^2 S^*, \tag{23}$$
$$\Pi_{xy}^*(S^*) = \frac{1}{N_\delta} \sqrt{\frac{3}{2}} \tan S^*,$$

where

$$S^* \equiv \sqrt{2/3} \varepsilon_{h_w} T_w^* s^*, \quad Y^* \equiv \sqrt{2/3} \varepsilon_{h_w} T_w^* y^*.$$

Note that, owing to the non-classical non-Navier law, the cross-stream pressure distribution is no longer uniform and normal stress has non-zero value. In the case of non-Navier non-Fourier laws, the constitutive equation of normal heat flux can be written

$$Q_y = \left(1 + \frac{\Pi_{yy}}{p} \right) \left(-k \frac{dT}{dy} \right) + \frac{ak}{pC_p} \Pi_{xy}. \tag{24}$$

The resulting temperature profile can be expressed as

$$T^*(S^*) = \cos^{-e} S^* \left[T^*(0) \right.$$
$$\left. - \frac{(\gamma - 1) \Pr T_w^{*3} M^2 \varepsilon_h^2}{192 N_\delta^2 (1 - e/4)} \frac{F(S^*)}{S_{1/2}^{*4}} \right] \tag{25}$$

where the function $F(S^*)$ is defined as

$$F(t) \equiv (4 - e) \left[\frac{1}{(4 - e) \cos^{4-e} t} \right.$$

$$-\frac{1}{(2-e)\cos^{2-e}t}-\left(\frac{1}{4-e}-\frac{1}{2-e}\right)\Bigg],$$

$$e=\frac{3(\gamma-1)}{2\gamma}.$$

With the temperature jump at the wall surface (15), the temperature profile can be determined as follows

$$T^*(S^*)=\cos^{-e}S^*\Big\{T^*(0)-\Big[T^*(0)$$

$$-\cos^e S_{1/2}^*\left(\alpha_T T_w^*+(1-\alpha_T)T^*(0)\right)\Big]\frac{F(S^*)}{F(S_{1/2}^*)}\Big\},$$

$$\alpha_T=\frac{\bar{\beta}_T p_w^*}{1+\bar{\beta}_T p_w^*},$$

(26)

and

$$\frac{\pi(\gamma-1)\,\text{Pr}\,\varepsilon_{h_w}^2 T_w^{*5}}{384\gamma\text{Kn}^2(1-e/4)}\frac{F(S_{1/2}^*)}{S_{1/2}^{*4}}=$$

$$T^*(0)\left(1-(1-\alpha_T)\cos^e S_{1/2}^*\right)-\alpha_T T_w^*\cos^e S_{1/2}^*.$$

(27)

The equation (27) is an algebraic equation of odd degree 5 with real coefficients. The unknown value T_w^* for given values of Kn and ε_{h_w} can be determined uniquely by using the bisection method. Interestingly, the tangential heat flux Q_x can exist from the constitutive relation of tangential heat flux

$$Q_x=\frac{\Pi_{xy}}{p}\left(-k\frac{dT}{dy}\right)+\frac{1}{\text{Pr}}\frac{(-\eta\,du/dy)}{p}Q_y$$

$$+\frac{ak}{pC_p}\Pi_{xx}.$$

(28)

The mass flow rate can then be expressed as

$$\frac{\dot{m}/2h}{\rho_r\sqrt{\gamma R T_w}}=\frac{\sqrt{\pi}}{16\sqrt{2\gamma}}\frac{T_w^{*2}}{u^*(0)}$$

$$\cdot\frac{\varepsilon_{h_w}}{\text{Kn}}\frac{(1-\alpha_V/3)}{\alpha_V}\left(\frac{\tan S_{1/2}^*}{2S_{1/2}^*}\right)^2,\quad \alpha_V=\frac{\bar{\beta}_V p_w^*}{1+\bar{\beta}_V p_w^*}.$$

(29)

3 Results and Discussion

Equations (5)-(21) represent a complete set of analytical solution for the Navier non-Fourier law. There exist three major shortcomings in the Navier non-Fourier law in comparison with more accurate non-Navier non-Fourier law. First, the normal stress Π_{yy} (or Π_{xx}) in (23) vanishes in the case of Navier law and, as a result, the kinematic stress constraint (22) does no longer exist. Second, the cross-stream pressure in the case of Navier law becomes uniform from the *y*-momentum equation in the conservation laws (4). Third, the tangential heat flux Q_x vanishes since the coupling term $a\Pi_{xx}$ in *x*-component of the constitutive equation of heat flux (28) disappears. Note that the first and second terms in the right-hand side of the constitutive equation of tangential heat flux (28) are of high order and therefore will disappear in the spirit of the linear Navier law.

On the other hand, the Navier non-Fourier theory turned out to be able to describe two other important features: the central temperature minimum and the Knudsen minimum in mass flow rate. This indicates that the force-stress coupling term, $a\Pi_{xy}$, in non-Navier non-Fourier constitutive relation (10) is solely responsible for the minimums in central temperature minimum profile and mass flow rate.
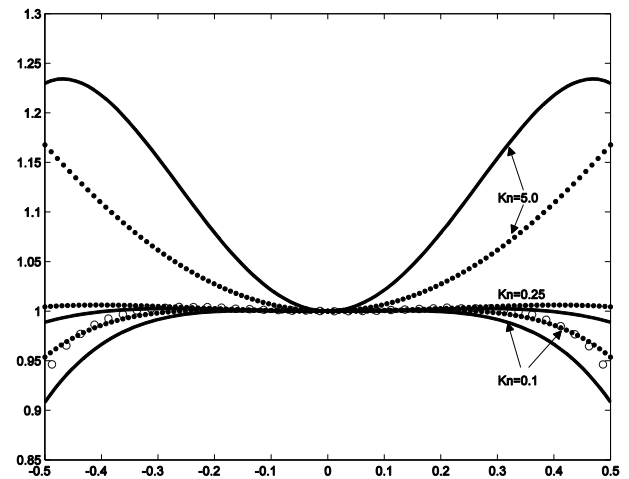
Fig. 2. Cross-stream temperature distribution $T(y^*)/T(0)$ in the force-driven compressible Poiseuille gas flow for various Knudsen numbers ($\varepsilon_{h_w}=0.6$). The solid line represents the compressible Navier non-Fourier result, while the ($\bullet$) and ($\circ$) symbols represent the non-Navier non-Fourier and DSMC (Kn=0.1; Uribe and Garcia, 1999) results.

The existence of the central temperature minimum is clearly shown in Fig. 2 for three Knudsen numbers 0.1, 0.25, 5.0. The low Knudsen number case (Kn=0.1) shows a temperature profile similar to the classical Navier-Fourier quartic function with a minimum at the center. Then around Kn=0.25 the temperature becomes almost uniform in whole domain. As the Knudsen number increases further, the central temperature minimum portion occupies all the domains, resulting in complete reversal of temperature profile; minimum at the center and maximum at the wall, in the case of Kn=5.0. This was possible by two effects: the force-stress coupling and the temperature jump at the wall. A difference is nonetheless found near the wall between Navier and non-Navier results for high Knudsen number because the Navier law cannot describe the concave pressure profile $p^*(S^*)=1+\tan^2 S^*$, which is the gist of the non-Navier theory.
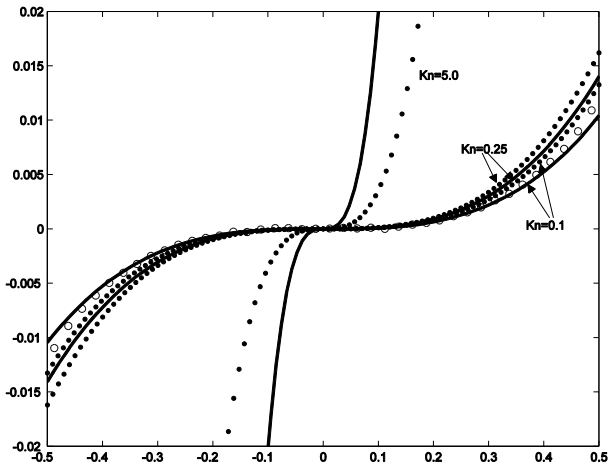
Fig. 3. Normal heat flux distribution $Q_y(y^*)/\left(hp^2(0)/\eta_w\right)$ in the force-driven compressible Poiseuille gas flow for various Knudsen numbers ($\varepsilon_{h_w}=0.6$). The solid line represents the compressible Navier non-Fourier result, while the ($\bullet$) and ($\circ$) symbols represent the non-Navier non-Fourier and DSMC (Kn=0.1) results.

Normal heat flux and stream-wise velocity profiles are also depicted in Figs. 3 and 4, respectively. The non-dimensional normal heat flux in general increases with an increasing Knudsen number. Both of Navier non-Fourier and non-Navier non-Fourier theories show

qualitatively similar results. The velocity profiles become more flat with an increasing Knudsen number owing to the increasing velocity slip at the wall. Again the difference between Navier non-Fourier and non-Navier non-Fourier results is shown to be small.
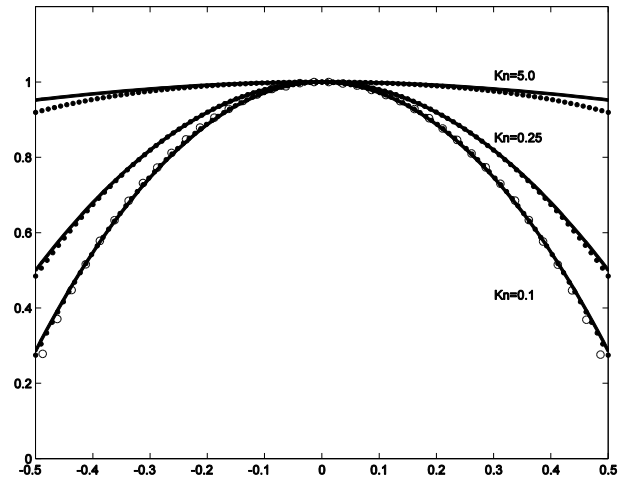
Fig. 4. Velocity distribution $u(y^*)/u(0)$ in the force-driven compressible Poiseuille gas flow for various Knudsen numbers ($\varepsilon_{h_w}=0.6$). The solid line represents the compressible Navier non-Fourier result, while the ($\bullet$) and ($\circ$) symbols represent the non-Navier non-Fourier and DSMC (Kn=0.1) results.
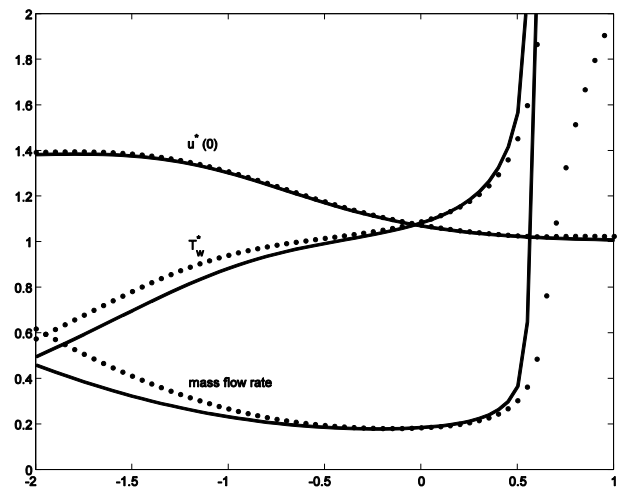
Fig. 5. Average velocity, average temperature, and mass flow rate $u(0)/u_r$, T_w/T_r, $\dot{m}/\left(2\rho_r h\sqrt{\gamma RT_w}\right)$ versus the Knudsen number in logarithmic scale in the force-driven compressible Poiseuille gas flow for various Knudsen numbers ($\varepsilon_{h_w}=0.6$). The solid line represents the compressible Navier non-Fourier result, while the ($\bullet$) symbols represent the non-Navier non-Fourier result.

Finally, the mass flow rate, along with the average temperature and the average velocity, are depicted with respect to the Knudsen number (from 0.01 to 10.0) in Fig. 5. Both theories predict a minimum in mass flow rate near Kn=1.0. Interestingly, it can be observed that this minimum is actually due to the average temperature T_w^{*2} appearing in equations of mass flow rate (20) and (29). This astonishing result means that the non-Fourier thermal law is solely responsible for the Knudsen minimum of mass flow rate in the present force-driven compressible Poiseuille gas flow, which is totally at odds with intuition obtained from conventional theory.

4 Conclusions

In this study, it was shown that two important exotic features in the force-driven compressible Poiseuille gas flow, non-uniform pressure distribution and non-zero normal stress, are due to the non-Navier law. In addition, the minimums in central temperature profile and mass flow rate are shown due to the force-stress coupling effect in non-Fourier law. Further it was shown that both of non-Navier and non-Fourier laws contribute to the existence of tangential heat flux.

In conclusion, the present study clearly demonstrates that non-classical thermal physics play a dominant role in gas flow far from thermal nonequilibrium and consequently thermal aspects of the problem must be treated very carefully. Even with isothermal wall condition, it was shown that the exotic temperature profile generated by the non-Fourier law is solely responsible for the Knudsen minimum in mass flow rate, which is totally against intuition. Further, theoretical and experimental investigation on the whole flowfields, such as cross-stream pressure and temperature distributions, beyond usual reduced quantities like the mass flow rate is needed to deeper understanding of micro- and nano-scale gas flows.

The present study is limited to the force-driven Poiseuille gas flow so that there may remain a question of whether the main results of non-classical thermal characteristics will carry over to non-Poiseuille configurations. Nevertheless, by considering the existence of non-classical cold-to-hot conductive heat flux in a micro-cavity gas flow (Mohammadzadeh et al., 2012), it is expected that most of non-classical results such as non-zero normal stress and tangential heat flux will hold in non-Poiseuille configurations as well.

Acknowledgements

References

Bhattacharya, D.K., Lie, G.C., 1989. Molecular-dynamics simulations of non-equilibrium heat and momentum transport in very dilute gases. Phys. Rev. Lett. 62, 897-900.

Chen, S., Tian, Z., 2007. Simulation of thermal micro-flow using lattice Boltzmann method with Langmuir slip model. Int. J. Heat Fluid Flow 31, 227-235.

Karniadakis, G., Beskok, A., Aluru, N., 2005. Microflows and Nanoflows: Fundamentals and Simulation. Springer.

Mansour, M.M., Baras, F., Garcia, A.L., 1997. On the validity of hydrodynamics in plane Poiseuille Flows. Physica A 240, 255-267.

Mohammadzadeh, A., Roohi, E., Niazmand, H., Stefanov, S., Myong, R.S., 2012. Thermal and second-law analysis of a micro- or nanocavity using direct-simulation Monte Carlo, Phys. Rev. E 85-5, 056310.

Myong, R.S., 2004. Gaseous slip model based on the Langmuir adsorption isotherm. Phys. Fluids 16-1, 104-117.

Myong, R.S., 2011. A full analytical solution for the force-driven compressible Poiseuille gas flow based on a nonlinear coupled constitutive relation. Phys. Fluids 23, 012002.

doi: 10.1063/1.3540671
http://acml.gnu.ac.kr/e-home/index.htm
(07/2014)

Myong, R.S., 2014. On the high Mach number shock structure singularity caused by overreach of Maxwellian molecules. Phys. Fluids 26-5, 056102.

Myong, R.S., Lockerby, D.A., Reese, J.M., 2006. The effect of gaseous slip on microscale heat transfer: An extended Graetz problem. Int. J. Heat Mass Trans. 49, 2502-2513.

Tij, R., Santos, A., 1994. Perturbation analysis of a stationary nonequilibrium flow generated by an external force. J. Stat. Phys. 76, 1399-1414.

Uribe, F.J., Garcia, A.L., 1999. Burnett description of plane Poiseuille flow. Phys. Rev. E 60, 4063-4078.

Veltzke, T., Thöming, J., 2012. An analytically predictive model for moderately rarefied gas flow. J. Fluid Mech. 698, 406-422.

Xu, K., 2003. Super-Burnett solutions for Poiseuille flow. Phys. Fluids 15-7, 2077-2080.

Zheng, Y., Garcia, A.L., Alder, B.J., 2002. Comparison of kinetic theory and hydrodynamics for Poiseuille flow. J. Stat. Phys. 109-3/4, 495-505.